

Extreme resonance line profile variations in the ultraviolet spectra of NGC 1624-2: probing the giant magnetosphere of the most strongly magnetized known O-type star

A. David-Uraz,^{1*} C. Erba,¹ V. Petit,¹ A. W. Fullerton,² F. Martins,³
 N. R. Walborn,^{2†} R. MacInnis,¹ R. H. Barbá,⁴ D. H. Cohen,⁵ J. Maíz Apellániz,⁶
 Y. Nazé,^{7‡} S. P. Owocki,¹ J. O. Sundqvist,⁸ A. ud-Doula,⁹ and G. A. Wade¹⁰

¹ *Department of Physics and Astronomy, University of Delaware, Newark, DE 19716, USA*

² *Space Telescope Science Institute, 3700 San Martin Drive, Baltimore, MD 21218, USA*

³ *LUPM-UMR 5299, CNRS & Université Montpellier, Place Eugene Bataillon, 34095 Montpellier Cedex 05, France*

⁴ *Departamento de Física y Astronomía, Universidad de La Serena, Av. Cisternas 1200 Norte, La Serena, Chile*

⁵ *Department of Physics and Astronomy, Swarthmore College, Swarthmore, PA 19081, USA*

⁶ *Centro de Astrobiología, CSIC-INTA. Campus ESAC. Camino bajo del castillo s/n. E-28 692 Villanueva de la Cañada. Spain*

⁷ *Université de Liège, Quartier Agora (B5c, Institut d'Astrophysique et de Géophysique), Allée du 6 Août 19c, B-4000 Sart Tilman, Liège, Belgium*

⁸ *Instituut voor Sterrenkunde, KU Leuven, Celestijnenlaan 200D, B-3001 Leuven, Belgium*

⁹ *Penn State Scranton, 120 Ridge View Drive, Dunmore, PA 18512, USA*

¹⁰ *Department of Physics and Space Science, Royal Military College of Canada, PO Box 17000, Stn Forces, Kingston, Ontario K7K 7B4, Canada*

Accepted 2018 November 23. Received 2018 November 21; in original form 2018 October 26

ABSTRACT

In this paper, we present high-resolution HST/COS observations of the extreme magnetic O star NGC 1624-2. These represent the first ultraviolet spectra of this archetypal object. We examine the variability of its wind-sensitive resonance lines, comparing it to that of other known magnetic O stars. In particular, the observed variations in the profiles of the CIV and SiIV doublets between low state and high state are the largest observed in any magnetic O-type star, consistent with the expected properties of NGC 1624-2's magnetosphere. We also observe a redshifted absorption component in the low state, a feature not seen in most stars. We present preliminary modelling efforts based on the Analytic Dynamical Magnetosphere (ADM) formalism, demonstrating the necessity of using non-spherically symmetric models to determine wind/magnetospheric properties of magnetic O stars.

Key words: stars: magnetic field – stars: early-type – stars: winds, outflows – stars: individual: NGC 1624-2 – ultraviolet: stars.

1 INTRODUCTION

Recent spectropolarimetric surveys such as the Magnetism in Massive Stars (MiMeS; Wade et al. 2016; Grunhut et al. 2017) and the B-fields in OB stars (BOB; Morel et al. 2015) projects have led to the establishment of a distinct population of massive stars hosting detectable magnetic fields at their surfaces. About 7% of Galactic OB stars are estimated to belong to this category.

Walborn (1972) identified a peculiar spectroscopic class of O stars with strong emission in their CIII $\lambda 4650$ line, comparable to that of the neighboring NIII lines, and labelled as “Of?p”. The most extreme example of this subclass is the O7f?p star NGC 1624-2 (Walborn et al. 2010). It has since been determined that this specific spectral feature (and various other observational properties of the Of?p stars) is an indication of magnetism (Grunhut et al. 2017). Indeed, all five Galactic Of?p stars host detectable fields, with NGC 1624-2 possessing the strongest known surface field of any O-type star by nearly an order of magnitude (~ 20 kG; Wade et al. 2012a).

Since the magnetic and rotational axes of a massive star

* E-mail: adu@udel.edu

† Deceased 22 February 2018.

‡ F.R.S.-FNRS Research Associate

are (in general) not aligned, rotational modulations arise, explaining the variability observed for these stars throughout the electromagnetic spectrum. In this context, spectropolarimetric timeseries provide information on the topology of the field, as the line-of-sight magnetic configuration varies with phase since we view a different portion of the stellar surface as the star rotates. The Oblique Rotator Model (ORM; Stibbs 1950) describes this effect for a large-scale dipolar magnetic field.

The H α emission of magnetic massive stars typically varies between a “low state” (corresponding to a nearly magnetic equator-on view) and a “high state” (pole-on view). NGC 1624-2 exhibits a single-wave variation of the equivalent width of H α over its rotational cycle (Wade et al. 2012a), suggesting that we only view a single magnetic hemisphere, assuming a dipolar field (see, e.g., Fig. 1 from Petit et al. 2015 for a schematic view of high and low state).

In most magnetic massive stars, a number of other observables are found to vary over the rotational period, in a way that is consistent with the ORM paradigm, such as the profiles of wind-sensitive UV resonance lines. UV observations are particularly important to diagnose the wind properties of massive stars (e.g., Pauldrach et al. 1994), as wind-sensitive resonance lines contain information about their structure and kinematics. UV properties have been studied for a few magnetic O stars: HD 37022 (= θ^1 Ori C; Stahl et al. 1996), HD 57682 (Grunhut et al. 2009, 2012), HD 148937 (Martins et al. 2012), HD 108 (Marcolino et al. 2012), HD 191612 (Marcolino et al. 2013), CPD -28 2561 (Nazé et al. 2015) and HD 54879 (Shenar et al. 2017).

The general phenomenology at UV wavelengths can be summarized as follows: at high state, strong lines show enhanced absorption at high velocities (compared to other rotational phases), while at low state, weaker lines exhibit strong low-velocity absorption (e.g., Nazé et al. 2015). As described below, they also show a departure from the line profiles expected for a spherically symmetric outflow, e.g., the Civ $\lambda\lambda 1548/50$ doublet is often found to be overall desaturated in the spectra of magnetic stars.

Magnetohydrodynamic (MHD) simulations have shown in great detail the process by which a magnetic field can confine the stellar wind into a circumstellar *magnetosphere* (ud-Doula & Owocki 2002). Slow rotators (such as NGC 1624-2, with a rotational period of 157.99d; Wade et al. 2012a) form *dynamical magnetospheres* (DMs), in which material flows along closed magnetic field loops from both magnetic hemispheres, colliding near the magnetic equator and then falling back onto the stellar surface, leading to complex and unstable flows.

Given its early spectral type, the dense stellar wind and extreme magnetic field of NGC 1624-2 interact strongly, creating a giant magnetosphere, much larger and denser than that of any other OB star. This is evidenced by the strong emission observed in its H α line (Wade et al. 2012a). In addition, the strong X-ray emission that is produced in magnetically confined wind shocks (MCWS) is substantially attenuated in NGC 1624-2, and varies with rotational phase (Nazé et al. 2014; Petit et al. 2015).

Because of its extreme properties, NGC 1624-2 constitutes the “Rosetta stone” of massive star magnetism. Despite its importance, there have been no UV observations of this unique object until recently. In this paper, we present

the first UV spectra of this object, obtained with the Cosmic Origins Spectrograph (COS) on the *Hubble Space Telescope* (HST).

In Section 2 we discuss the observations. Section 3 offers a qualitative description of the spectra and compares NGC 1624-2 to other non-magnetic and magnetic stars of similar spectral type. In Section 4 we describe our preliminary modelling methods and show some early results, including a comparison of NGC 1624-2’s resonance line profiles to synthetic lines computed using the Analytic Dynamical Magnetosphere (ADM) formalism of Owocki et al. (2016). Finally, in Section 5 we draw conclusions and discuss future work.

2 OBSERVATIONS

Ultraviolet spectra of NGC 1624-2 were obtained at two rotational phases with the Cosmic Origins Spectrograph (COS) on board the *Hubble Space Telescope*. The spectra were acquired near phases corresponding to the “high” ($\phi \sim 0.0$) and “low” ($\phi \sim 0.50$) states of the H α variations. Table 1 provides a journal of these observations, which constitute *HST* General Observer Program 13734 (PI: Petit).

For each visit, the data were collected with COS over two consecutive orbits. The first orbit was devoted to a target acquisition in the bright object aperture (BOA), which is required to place NGC 1624-2 accurately in the circular primary science aperture (PSA; 2.5” diameter). The target acquisition was followed by two exposures with the G130M grating centered on wavelengths of 1291 and 1327 Å, respectively. During the second orbit, exposures with the G160M grating centered on wavelengths of 1577 and 1623 Å were obtained. These combinations provided complete wavelength coverage from about 1130 to 1800 Å with a resolving power that increases linearly with wavelength from 16,000 to 21,000 over the respective ranges of both gratings. At each grating setting, the exposure was divided into 4 sub-exposures of equal duration but different FP-POS positions to mitigate the effects of fixed-pattern noise in the combined spectrum. All observations were obtained in time-tag mode by using both channels of the FUV cross-delay (XDL) line detector.

The spectra were uniformly processed with version 3.0 (2014 October 30) of the CALCOS calibration pipeline. The steps included: correcting the photon-event table for dead-time and positional effects such as drifts in the detector electronics, geometric distortion, and the Doppler shift of the observatory; binning the time-tag data and assigning wavelengths to the bins on the basis of Pt-Ne spectra acquired simultaneously with spectra of NGC 1624-2; extraction and photometric calibration of 1-D spectra; and the “shift and add” combination of spectra taken at different FP-POS positions of individual grating settings. Since the first spectra of NGC 1624-2 were obtained shortly after the move to life-time adjustment position 3 was implemented (on 2015 February 9), special care was taken to process the data with the appropriate reference files. Fiducial values of the signal-to-noise ratio (S/N) per 9-pixel resolution element are indicated in Table 1. These estimates were computed from the mean flux between 1350 and 1355 Å and 1490 and 1495 Å for the settings of the G130M and G160M gratings, respectively. Since these intervals contain weak spectral features,

the pixel-to-pixel noise was estimated from the scatter in the difference between the processed flux vector and a version that was smoothed over a resolution element.

Finally, the IDL procedure `coadd_x1d`¹ was used to merge the extracted, calibrated spectra into a single spectrum.

3 COMPARISON TO STARS OF SIMILAR SPECTRAL TYPE

The UV spectra of NGC 1624-2 are shown in Figure 1. The low-state spectrum is shown in pink and the high-state spectrum is shown in blue.

3.1 Qualitative description of the main UV spectral features of NGC 1624-2 and comparison with non-magnetic O stars

We first note that some of the most prominent spectral features undergo large variations over time. In particular, two important wind-sensitive resonance line doublets (SiIV $\lambda\lambda 1393/1402$ and CIV $\lambda\lambda 1548/50$) show clear differences in their line profiles between both phases due to rotational modulation as the viewing angle of the magnetosphere changes.

There is more absorption overall during the low state than during the high state. This is expected, since when the magnetosphere is viewed equator-on, there is a large amount of confined material obscuring the stellar disk. However, despite the overall absorption being stronger, we can see that for the CIV doublet, the high-velocity, blue-shifted absorption is actually stronger during the high state. The emission peak of the doublet remains at roughly the same level at both phases for CIV, but in the case of SiIV, the overall emission is clearly stronger during the high state.

Fig. 2 compares the profiles of NGC 1624-2's main wind-sensitive lines with those of two non-magnetic stars of similar spectral type: O7V((f))z (HD 93146, top) and O8III((f)) (HD 36861, bottom).

Comparing NGC 1624-2 with the dwarf O-type star HD 93146², we find that they both show similarly desaturated absorption troughs in their CIV doublet. The blue edge of the line profile of NGC 1624-2 appears at a lower velocity than that of the non-magnetic star, and in fact suggests a terminal velocity that is significantly lower than what is theoretically expected (2875 km s^{-1} ; Wade et al. 2012a). However the emission component of NGC 1624-2 is stronger.

On the other hand, while the absorption trough of the CIV doublet in the O giant HD 36861 is strongly saturated,

its emission still is not as strong as that exhibited by NGC 1624-2.

Finally, when compared to both stars, NGC 1624-2's SiIV doublet stands out as it presents a fundamentally different morphology. In both non-magnetic stars, it is essentially unaffected by the wind, as is to be expected for a late O star. However, we can see a clear P Cygni-like profile in NGC 1624-2 during the low state. The double-peaked emission morphology present at the high state is to date unique to NGC 1624-2 and could arise from low-velocity material near the magnetic equator flowing from both magnetic hemispheres (therefore some material has a positive net line-of-sight velocity while the other half has a negative velocity), just off the limb of the star as it is viewed pole-on.

3.2 Comparison with other magnetic O-type stars

In Fig. 3, we visually compare the main wind-sensitive features of NGC 1624-2's spectra (namely the aforementioned SiIV and CIV doublets) to those of 7 other magnetic O stars for which archival UV spectra are available (though not always at extreme phases; blue lines denote high-state spectra and pink lines denote low-state spectra, while grey lines correspond to all other phases). The stellar and magnetospheric properties of these stars are summarized in Table 2, and details regarding the observations can be found in the Appendix.

The first obvious observation is that the resonance line profiles of NGC 1624-2 exhibit a much more pronounced variability than that of the comparison stars. This can undoubtedly be understood in terms of its larger and denser magnetosphere. Furthermore, as it is viewed nearly pole-on at high-state and nearly equator-on at low-state, we can probe roughly the full range of possible viewing angles. Its field configuration thus yields the greatest possible variability given its magnetospheric parameters, along with perhaps CPD -28 2561 and HD 57682 (for which both poles can presumably be seen over a rotational cycle, as suggested by their double-wave H α variations; see Table 2).

At its low state, NGC 1624-2's SiIV doublet shows a clear P-Cygni profile which is more reminiscent of an early-type O giant, or an OB supergiant. Among other magnetic O stars, only HD 108 shows a similar emission. However, it does not share the remarkable double-peaked emission morphology that NGC 1624-2 exhibits in its high state. The other stars mostly exhibit minor variations of this doublet, with a slight broadening and more absorption at low state.

In contrast, the CIV doublet of NGC 1624-2 shows less absorption at high velocity during the low state, but more absorption at low velocity (which also manifests as an apparent decrease of the red-shifted emission). This is consistent with synthetic lines computed from MHD simulations (Marcolino et al. 2013), and similar to the variation seen in CPD -28 2561.

Another interesting feature of NGC 1624-2's UV resonance lines is the presence of broad, red-shifted absorption at low-state in both doublets. Among the other magnetic O stars, this feature is only seen in HD 54879, and could be linked to infalling material. In fact, HD 54879's UV spectrum is surprisingly similar to NGC 1624-2's low-state spectrum, despite its later spectral type.

Finally, we can also see from Fig. 1 that the absorption

¹ This procedure was developed by the COS Instrument Definition Team. See Danforth et al. (2010) for a description and a hyperlink to the software repository.

² Two components are known, HD 93146A and HD 93146B (O9.7IV; Sota et al. 2014), although it is not known whether they are physically bound. This might even be a hierarchical triple system (Mayer et al. 2017), but in any case, the light is dominated by the primary. While the other components could fill the line profile slightly, contributing to its desaturation (in the case of the CIV doublet), this profile appears consistent with that of other stars of similar spectral type (Walborn et al. 1985).

Table 1. Journal of COS Observations

ObsID	Grating	λ_c^1 (Å)	S/N	UT (Start)	Exp. Time (s)	MJD(mid)	ϕ^2
lcl601010	G130M	1291	15.8	2015-02-17T06:16:42	848	57070.2685	0.986
lcl601020	G130M	1327	14.8	2015-02-17T06:39:53	844	57070.2846	0.986
lcl601030	G160M	1577	22.9	2015-02-17T07:40:05	1084	57070.3279	0.986
lcl601040	G160M	1623	22.6	2015-02-17T08:07:48	1080	57070.3472	0.986
lcl602010	G130M	1291	16.9	2015-10-06T16:20:53	848	57301.6881	0.451
lcl602020	G130M	1327	15.0	2015-10-06T16:44:04	844	57301.7042	0.451
lcl602030	G160M	1577	21.6	2015-10-06T17:07:58	1084	57301.7309	0.451
lcl602040	G160M	1623	21.1	2015-10-06T18:00:30	1080	57301.7588	0.452

¹ Central wavelength of the grating setting.

² Phase of MJD(mid) according to the ephemeris of Wade et al. 2012a.

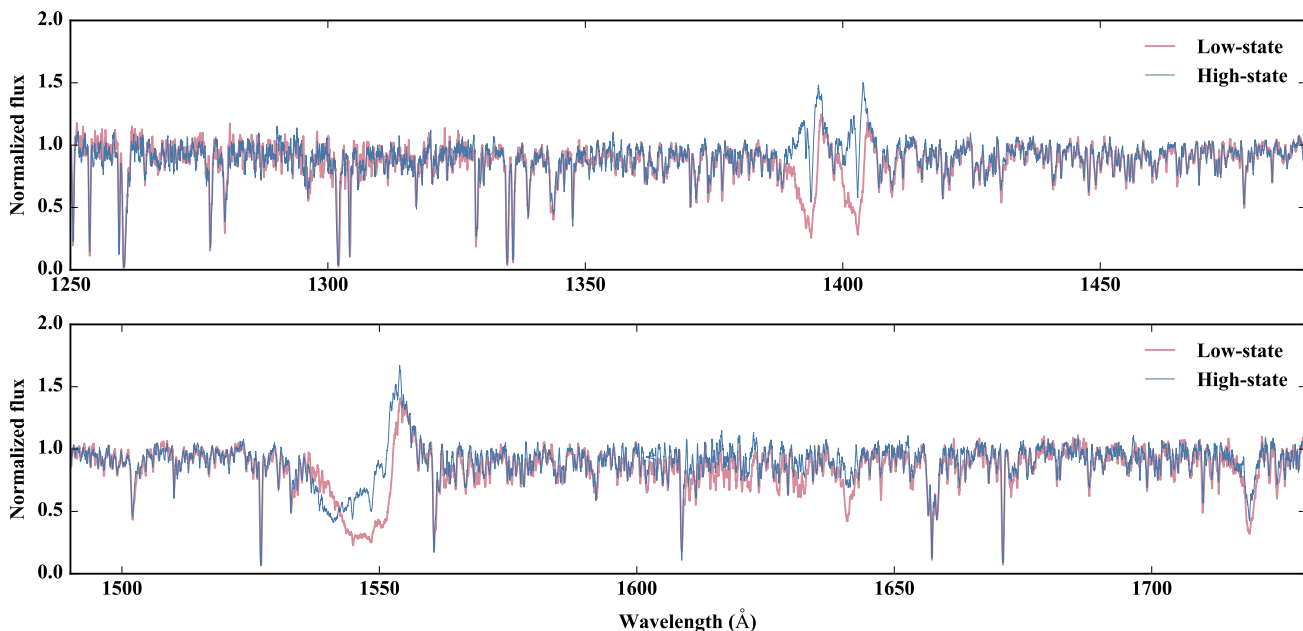


Figure 1. *HST* observations of NGC 1624-2 (high-state in blue, low-state in pink) smoothed with an 11-pixel wide boxcar filter for display purposes. There are important variations in both the SiIV $\lambda\lambda$ 1393/1402 and CIV $\lambda\lambda$ 1548/1550 doublets, as well as a modulation of the strength of the absorption in the FeIV “forest” around 1615-1630Å.

in the “forest” of FeIV photospheric lines is modulated between phases, appearing to be stronger at low state. This behaviour was also observed in the cases of HD 108 and HD 191612 (Marcolino et al. 2013).

As was pointed out by Nazé et al. (2015), comparing the behaviour of the UV resonance lines of all observed magnetic O stars (with the exception of HD 37022, which puzzlingly seems to exhibit the exact opposite behaviour; see section 4.1) leads to an overall consistent phenomenology for the variations seen in the UV wind-sensitive lines of magnetic O stars. In the case of *strong*³ lines, which can probe low-density, high-velocity material further from the stellar surface, the P-Cygni characteristics of the line profile seem to be intensified at high state. On the other hand, *weak* lines are formed in regions of high density, that can provide enough optical depth despite their weak opacity; these high-

density regions are usually found surrounding the magnetic equator, closer to the star and therefore contribute significant low-velocity absorption at low state.

This means that there are two main factors in understanding the nature and amplitude of the line profile variations detected in UV lines: line strength and the range of magnetospheric viewing angles. As further discussed in the following section, the line strength itself depends sensitively on the ionization balance and the mass-loss rate (or in the case of magnetic massive stars, the wind-feeding rate as discussed below). This can explain the range of behaviours and line morphologies examined in this subsection. As for the viewing angle, it appears that the extremes of these line profile variations correspond to a pole-on view ($\alpha = 0^\circ$) and an equator-on view ($\alpha = 90^\circ$), so a larger range in viewing angle between those two values will lead to larger variations. Conversely, for HD 148937, the limited range in viewing angle precludes sampling the full range of variations. Finally, depending on how far from the surface a wind-sensitive line

³ In other words, lines which correspond to electronic transitions with a large opacity.

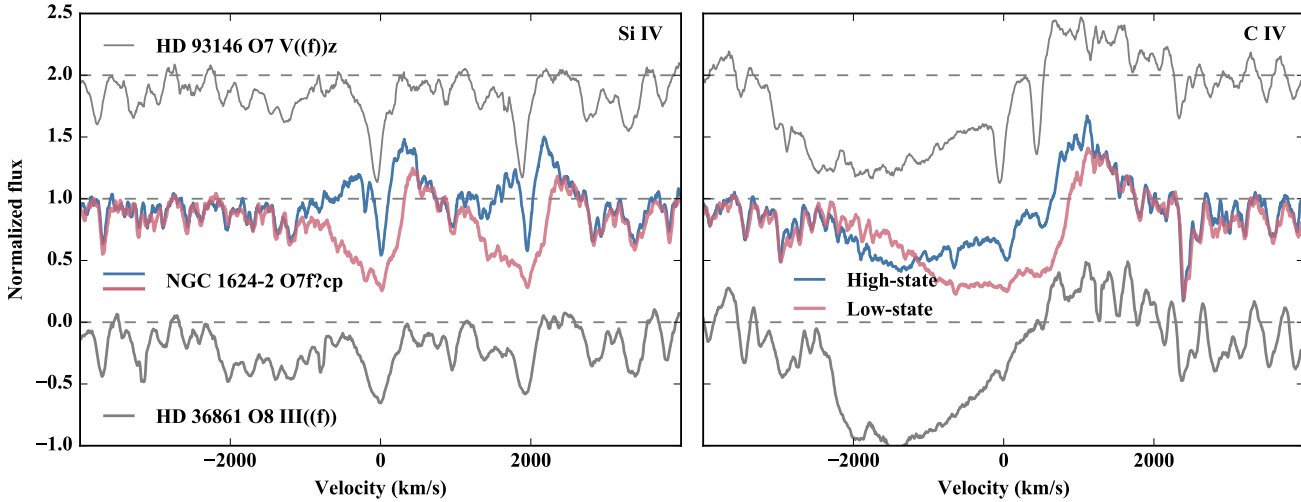


Figure 2. Comparison between the resonance line profiles of NGC 1624-2 and that of non-magnetic stars of similar spectral type (SiIV $\lambda\lambda 1393/1402$ on the left and C IV $\lambda\lambda 1548/50$ on the right). The velocity axes refer to the blue component of the doublets. We see important differences in the morphologies of these lines, suggesting that the wind structure of NGC 1624-2 shows a strong departure from spherical symmetry.

Table 2. List of magnetic O-type stars appearing in Fig. 3 with their stellar and magnetospheric properties: effective temperature (T_{eff}), mass (M_*), luminosity (L), mass-driving rate ($\dot{M}_{B=0}$), as calculated using the theoretical prescription by Vink et al. (2001), dipolar field strength (B_p), inclination angle (i ; the angle between the rotation axis and the line of sight), the obliquity angle (β ; the angle between the magnetic field axis and the rotation axis) and the range of viewing angles (α ; the angle between the magnetic field axis and the line of sight). References for the stellar and magnetic parameters are the following: *a*) Wade et al. (2012a); *b*) Martins et al. (2010); *c*) Shultz & Wade (2017); *d*) Martins et al. (2012); *e*) Howarth et al. (2007); *f*) Wade et al. (2011); *g*) Wade et al. (2015); *h*) Walborn et al. (2010); *i*) Simón-Díaz et al. (2006); *j*) Wade et al. (2006); *k*) Grunhut et al. (2009); *l*) Grunhut et al. (2012); *m*) Nazé et al. (2008); *n*) Wade et al. (2012b); *o*) Shenar et al. (2017); *p*) Castro et al. (2015) and *q*) Sota et al. (2011).

Star Spectral type	T_{eff} (kK)	M_* (M_\odot)	$\log(L)$ (L_\odot)	$\log(\dot{M}_{B=0})$ ($M_\odot \text{yr}^{-1}$)	B_p (kG)	i ($^\circ$)	β ($^\circ$)	α range ($^\circ$)
NGC 1624-2 O7f?cp ^a	35 ± 2 ^a	~ 30 ^a	5.2 ± 0.1 ^a	-6.8	~ 20 ^a	$\lesssim 45$ ^a	$\lesssim 45$ ^a	$\sim 0 - 90$
HD 108 O4-8f?p ^d	35 ± 2 ^b	42 ± 5 ^c	5.7 ± 0.1 ^b	-5.55	≥ 1.15 ^c	N/A	N/A	N/A
HD 191612 O6-8f?p ^d	35 ± 1 ^e	~ 30 ^e	~ 5.4 ^e	~ -6.0	2.45 ± 0.40 ^f	~ 30 ^f	67 ± 5 ^f	$\sim 37 - 97$
CPD -28 2561 O6.5f?p ^h	35 ± 2 ^g	61 ± 33 ^g	5.35 ± 0.15 ^g	-6.56	2.6 ± 0.9 ^g	35 ± 3 ^g	90 ± 4 ^g	$\sim 55 - 125$
HD 37022 O7V ^d	39 ± 1 ⁱ	45 ± 16 ⁱ	5.31 ± 0.13 ⁱ	-6.40	1.525 ± 0.375 ^j	45 ± 20 ^j	$\sim 48 \pm 20$ ^j	$\sim 3 - 93$
HD 57682 O9IV ^d	34.5 ± 1.0 ^k	17_{-9}^{+19} ^k	4.79 ± 0.25 ^k	-7.08	0.88 ± 0.05 ^l	~ 60 ^l	79 ± 4 ^l	$\sim 19 - 139$
HD 148937 O5.5-6f?p ^d	41 ± 2 ^m	~ 60 ⁿ	5.8 ± 0.1 ⁿ	~ -5.5	$1.02_{-0.38}^{+0.31}$ ⁿ	$\lesssim 30$ ⁿ	38_{-28}^{+17} ⁿ	$\sim 8 - 68$
HD 54879 O9.7V ^q	30.5 ± 0.5 ^o	14 ± 7 ^o	4.45 ± 0.20 ^o	-7.9	≥ 2 ^p	N/A	N/A	N/A

is formed, it might be more or less affected by magnetic wind confinement depending on the Alfvén radius.

4 MODELLING

4.1 Previous modelling efforts

In non-magnetic stars, UV resonance lines provide a critical diagnosis of wind properties. Spectral synthesis codes such as CMFGEN (Hillier & Miller 1998) use models with spherically symmetric winds. Therefore, fitting the UV spectrum

of a non-magnetic massive star with one of these models yields the mass-loss rate and terminal velocity of the wind.

However, the picture is more complicated in a magnetic massive star, since the field impacts both the density and velocity distribution of the circumstellar material, reshaping the wind into a magnetosphere. The usual assumption to circumvent this issue has been to consider, whenever possible, the high state spectrum to perform a quantitative spectral analysis using spherically symmetric models. Close to the magnetic pole the wind breaks open the field lines and the flow is nearly radial; therefore this viewing angle shows us

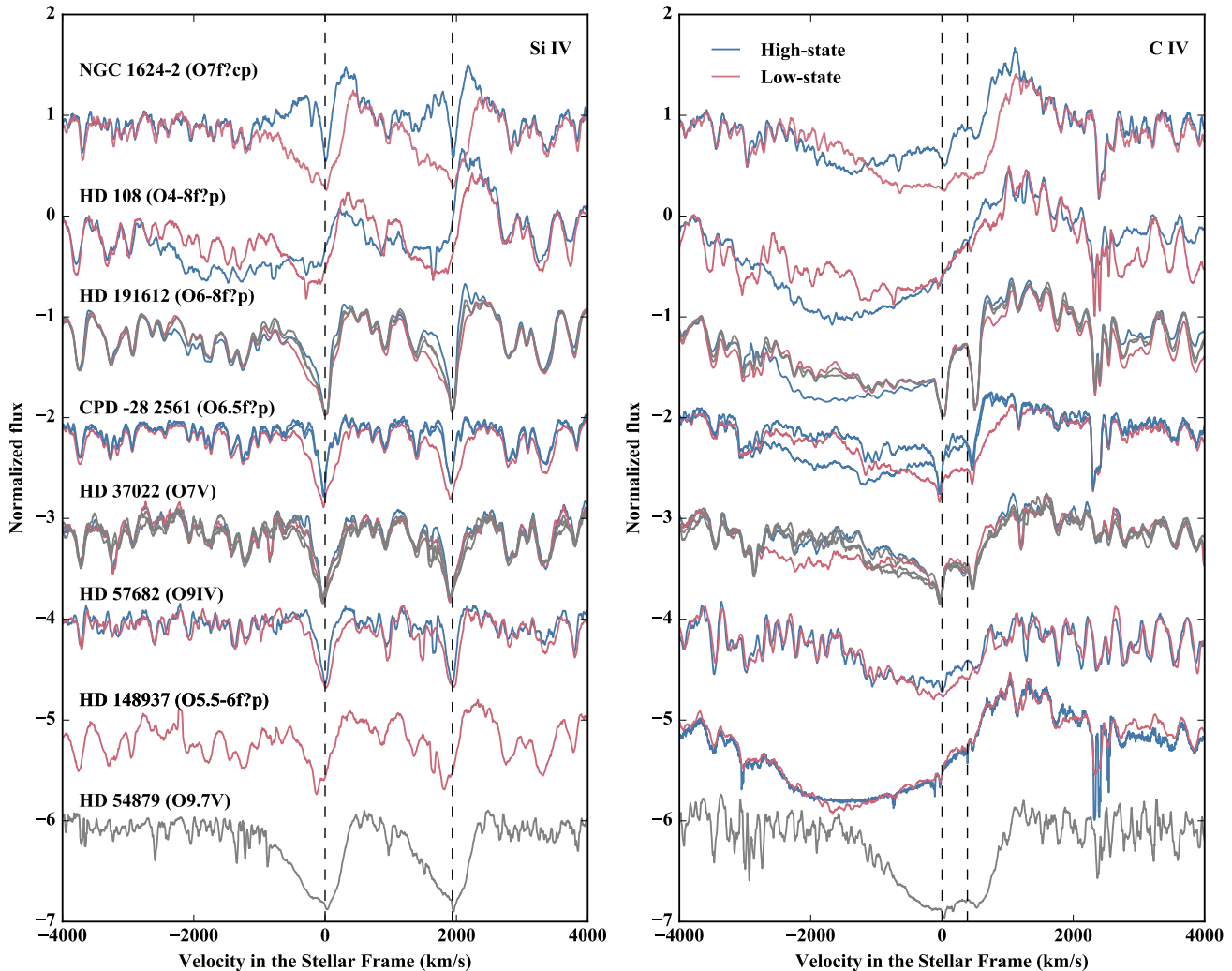


Figure 3. Comparison between the resonance line profiles of NGC 1624-2 and that of other magnetic O-type stars. The velocity axis is centered on the position of the blue component of the doublet.

the part of the magnetosphere that most resembles a spherically symmetric wind.

Such an approach has been adopted using CMFGEN in the cases of HD 108 (Marcolino et al. 2012), HD 191612 (Marcolino et al. 2013) and HD 57682 (Grunhut et al. 2009), and using the PoWR code (Gräfener et al. 2002; Hamann & Gräfener 2003) in the case of HD 54879 (Shenar et al. 2017). However, these attempts were typically not able to account for the detailed shapes of the line profiles and yielded mass-loss rates that are at least an order of magnitude lower than the expected theoretical rates. In the case of HD 57682, Grunhut et al. (2012) used a heuristic model with a disc of circumstellar material concentrated around the magnetic equator to reproduce the observed variations in the $H\alpha$ emission. This model yielded a mass-loss rate which was between 10 and 30 times greater than that inferred from the previous CMFGEN fit to the UV spectrum.

Spherically symmetric models can also be used to determine the ionization balance in the wind. This approach was used for instance by Nazé et al. (2015) for CPD -28

2561, using FASTWIND (Puls et al. 2005, combined with a new X-ray treatment implemented by Carneiro et al. 2016).

It has been shown that the behaviour of the UV resonance lines of magnetic O stars can be qualitatively understood by performing radiative transfer through MHD simulations. This technique has proven successful for both HD 191612 (Marcolino et al. 2013) and CPD -28 2561 (Nazé et al. 2015). In the former case, the opposite behaviours of the C IV and Si IV doublets is properly reproduced. For the latter star, MHD simulations coupled with a TLUSTY photospheric profile (Lanz & Hubeny 2003) and radiative transfer can reproduce the observed broadening of the Si IV doublet's absorption at low state.

However, MHD simulations fail to reproduce the observed variability of HD 37022, showing instead an offset of 0.5 in rotational phase (ud-Doula 2008). While this could perhaps be understood in terms of certain hypotheses formulated by Stahl et al. (1996) regarding the magnetic field topology (well before the field was even detected), further magnetic characterization of this star by Wade et al.

(2006) conclusively excludes this possibility, making this phenomenology an enduring puzzle.

4.2 Departure from spherically symmetric winds

Wade et al. (2012a) used the optical spectrum of NGC 1624-2 to derive its stellar properties, and then computed a mass-loss rate of $1.6 \times 10^{-7} M_{\odot} \text{yr}^{-1}$ using the prescription by Vink et al. (2001). However, it is important to note that this corresponds to the value the mass-loss rate would have if the star did not possess a magnetic field, or in other words the *wind-feeding rate*, $\dot{M}_{B=0}$. The parameterizations derived by, e.g., ud-Doula & Owocki (2002); ud-Doula et al. (2008, 2009) to describe various quantities related to massive star magnetospheres (such as the confinement parameter, spin-down time and Alfvén radius) are also all expressed in terms of the wind-feeding rate.

In reality, however, this wind-feeding rate does not correspond to the total surface mass flux, since the local mass flux varies latitudinally due to the inclination of the magnetic field with respect to the normal to the stellar surface (Owocki & ud-Doula 2004). This leads to a reduction of the integrated surface mass flux by a factor of nearly one-half in the case of a pure dipole (Owocki et al. 2016). Furthermore, the magnetic field confines a large portion of the outflowing material (up to 96% in the case of NGC 1624-2), which means that the “real” mass-loss rate should only take into account the material that actually escapes the star, mostly the outflow around the polar region that is not confined (e.g., ud-Doula et al. 2008; Petit et al. 2017). This “real” mass-loss rate is of particular interest in the context of stellar evolution modelling (e.g., Petit et al. 2017; Keszthelyi et al. 2017; Georgy et al. 2017).

To recapitulate, we are distinguishing between three main quantities:

- (i) the “wind-feeding rate” (or $\dot{M}_{B=0}$) which corresponds to the expected mass-loss rate (in our case obtained via a theoretical prescription) a non-magnetic star with the same stellar parameters would have;
- (ii) the integrated surface mass flux, which, compared to the previous quantity, is reduced by some factor due to the inclination of the surface magnetic field lines; and
- (iii) the “real” mass-loss rate, which corresponds to the material escaping both the star’s gravity and the magnetic confinement along open field lines.

The question then becomes which one (if any) of these rates would UV line fitting yield? Ideally, we would like to use a model that, taking into account the magnetospheric geometry, would recover $\dot{M}_{B=0}$. First, we consider, as has been done traditionally, the case of a spherically symmetric model.

We compute CMFGEN models using the unclumped wind-feeding rate ($\log \dot{M}_{B=0} = -6.8$) adopted by Wade et al. (2012a) as well as an equivalent clumped wind-feeding rate of $\log \dot{M}_{B=0} = -7.3$ using a typical (e.g., Figer et al. 2002) volume-filling clumping factor of $f = 0.1$ (since $\dot{M} \propto \sqrt{f}$ for optically thin clumping). We also take into

account the X-ray luminosity⁴ ($L_X/L_{\text{bol}} = -6.2$) obtained by Petit et al. (2015). Finally, we compare these models to our high-state spectrum. The agreement with the wind features is poor (see section 4.5), as expected, and we find that any attempt to fit the blue-shifted absorption of UV resonance lines would yield a wind-feeding rate at least one order of magnitude lower than the theoretical value (as has been found for other stars). This is due in part to the faster-than-radial expansion of a radial polar flow tube in a magnetic wind (e.g., Kopp & Holzer 1976; Owocki & ud-Doula 2004), as discussed by Marcolino et al. (2013).

However, if we focus on photospheric lines, such as the Fev and FeIV “forests”, we notice some interesting features. In Fig. 4 we show the associated regions in the (high-state) spectrum. Thin black lines are models for various combinations of microturbulent velocity (v_{turb}) and metallicity (and thus iron content). The effective temperature and surface gravity are those determined by Wade et al. (2012a) based on the analysis of the optical spectrum. A standard model with solar composition (Z_{\odot}) and a microturbulent velocity of 10 km/s produces too much FeIV absorption. Reducing v_{turb} to 3 km/s (middle) improves the fit but the FeIV absorption remains too strong. Further reducing v_{turb} to 1 km/s (not shown) does not change this picture significantly. On the other hand, reducing only the metallicity with a fixed microturbulent velocity of 10 km/s (top) does not reduce the strength of the FeIV absorption sufficiently to reproduce the observed spectrum. However, a model with a metallicity of $Z_{\odot}/5$ and with $v_{\text{turb}} = 3$ km/s (bottom) simultaneously reproduces the absorption strength of both the Fev and FeIV “forests”. Such a fit could not be accomplished by changing, e.g., the surface temperature, since that would also affect the depth of the Fev “forest”, thus simply shifting the problem from one set of lines to the other. We note that Sundqvist et al. (2013) reported the suppression of turbulent broadening in NGC 1624-2 as observed in the optical spectra.

Taking into account a lower metallicity should lead to a lower theoretical wind-feeding rate (by roughly half an order of magnitude). However, while this result is intriguing, a proper abundance analysis for a magnetic O star would benefit from using non-spherically-symmetric atmospheric models (as evidenced by, e.g., the modulation of the FeIV forest between high and low state). Since such models are not currently available, we limit ourselves to noting the possibility of a subsolar metallicity⁵, while still using the theoretical mass-loss rate computed at solar metallicity by Wade et al. (2012a) for our subsequent modelling and analysis.

4.3 Magnetospheric modelling

While it is possible to use MHD simulations to model massive star magnetospheres, they involve expensive calculations. Therefore, they are not particularly well suited to model a set of magnetic stars with various stellar and magnetic parameters. Furthermore, such calculations are

⁴ Based on a fit to an ISM-corrected model for NGC 1624-2 in its high state.

⁵ There have been no metallicity measurements for the cluster NGC 1624, but its position at the edge of the Galactic disk could be consistent with a subsolar value.

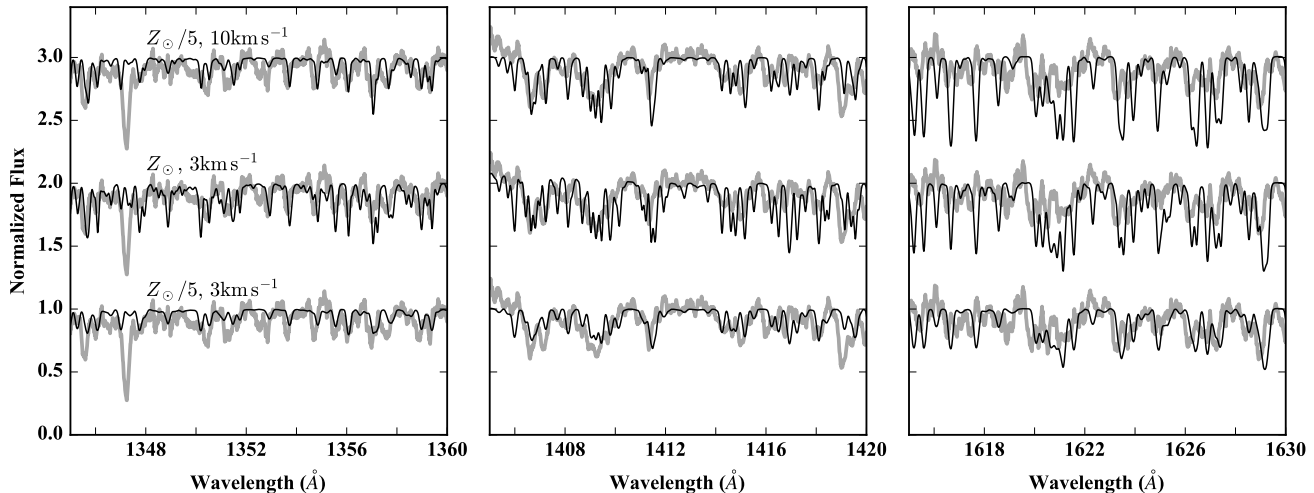


Figure 4. Fev (left and middle panel) and FeV (right panel) “forests” of photospheric lines. The high-state observation is represented by the thick grey lines and the models by the thin black lines. The observation is compared to the best fit CMFGEN model on the bottom, which uses both subsolar metallicity and low microturbulent velocity, and to two other models which implement each of these factors separately in the middle and on the top (vertically offset by 1 and 2, respectively). Only the model on the bottom can simultaneously match the line strengths for all three “forests”.

not practical for a star like NGC 1624-2, due to its extremely strong magnetic field that leads to a high Alfvén speed, and consequently to extremely short Courant stepping times. In contrast, the simplified parameterizations included in the ADM formalism provide a significantly more efficient method to model the time-averaged behaviour of this star’s magnetosphere and might allow us to recover its wind-feeding rate. This method has already been shown to successfully reproduce the H α variations of slowly rotating magnetic massive stars (Owocki et al. 2016).

The ADM model consists of three main components. The *upflow* is the ionized material radiatively driven from the surface of the star. The ADM formalism makes the assumption that the magnitude of the material’s velocity follows a β -law⁶, but that its direction follows that of the field lines, as the material flows along the closed field loops from both magnetic hemispheres. This upflow leads to a region of shocked plasma, located between the shock front and the apex of the magnetic loop, close to the plane of the magnetic equator leading to a region of *hot post-shock gas*, whose extent depends on the cooling efficiency. Finally, once cooled, the material simply forms a *downflow* that starts at the loop apex and flows back onto the surface of the star along the field loops, undergoing free fall. Of course, the simultaneous presence of these three components at a given point in space is not physical, but it represents an adequate time-averaged picture of the dynamic flows which occur within the magnetosphere. Given these three components, the ADM model provides us with analytical prescriptions for the density and velocity at each point within the magnetosphere.

To model NGC 1624-2’s magnetosphere, we make a few simplifying assumptions and approximations. We first con-

sider a pure dipole model with an infinite Alfvén radius⁷ (R_A). In reality, for NGC 1624-2, $R_A \approx 11.4R_*$, which is large enough for this approximation to be warranted, since the extremely low densities at that distance will not contribute much to the line of sight optical depth. The extent of the closed field loops in NGC 1624-2’s magnetosphere also eliminates concerns that the ADM poorly reproduces the outer wind (Hennicker et al. 2018)⁸.

Furthermore, for this initial investigation, we only consider the upflow component. This is because we are seeking to investigate the desaturation that occurs within the high-velocity absorption trough in the high state. Since the downflow component located between the stellar disk and the observer (looking pole-on) would be redshifted, and the shock-heated region also should not cross the stellar disk from the observer’s perspective (unless the cooling is unrealistically inefficient), using only the upflow provides a proof of concept to test whether the ADM formalism offers a better basis than previous methods to provide a quantitative estimate of the wind-feeding rate.

4.4 Radiative transfer

To perform radiative transfer on our model magnetosphere, we use a variation of the Sobolev with Exact Integration (SEI) method for a singlet (Hamann 1981; Lamers et al. 1987), taking into account the κ_0 formalism of line strength as presented by Sundqvist et al. (2014) (their eq. 13). This parameter is proportional to the mass-loss rate and the fractional abundance of the absorbing ion for a given line.

⁶ And in particular in this case, a velocity law using $\beta = 1$ such that the radial dependence of the velocity follows $v(r) = v_\infty(1 - R_*/r)$.

⁷ In a dipole model, the Alfvén radius corresponds roughly to the radius of closure of the largest closed field loop.

⁸ This particular study used HD 191612, with a much smaller Alfvén radius of $2.7R_*$, to compare MHD simulations and the ADM formalism using, in effect, an infinite Alfvén radius.

The scalings used in the ADM model take into account two important velocities: the terminal velocity of the wind, v_∞ , and the escape velocity,

$$v_e \equiv \sqrt{\frac{2GM_*(1-\Gamma_e)}{R_*}} \quad (1)$$

where G is the universal gravitational constant, M_* and R_* are the stellar mass and radius, respectively, and

$$\Gamma_e \equiv \frac{\kappa_e L}{4\pi GM_* c} \quad (2)$$

is the standard Eddington factor, with $\kappa_e = 0.34 \text{ cm}^2 \text{ g}^{-1}$, the Thomson electron scattering opacity and c , the speed of light. Finally, we define

$$\gamma_w \equiv v_\infty / v_e \quad (3)$$

to be the ratio between the terminal and escape velocities. Generally, for stars on the hot side of the bi-stability jump ($T_{\text{eff}} \gtrsim 21 \text{ kK}$), it is assumed that $\gamma_w = 2.6$ (Lamers et al. 1995).

Then, for a given frequency within the line profile w_{obs} , expressed in terms of velocity (normalized to v_∞), we obtain the following expression for an infinitesimal element of optical depth for a point along the line-of-sight (z) direction:

$$d\tau(w_{\text{obs}}, z) = \frac{\kappa_0 \gamma_w}{\sqrt{\pi} w_D} \frac{\rho}{\rho_{c*}} \exp\left[-\left(\frac{w_z - w_{\text{obs}}}{w_D}\right)^2\right] dz \quad (4)$$

where w_D is a velocity broadening parameter taking into account both thermal and turbulent velocity fields (in units of v_∞ ; for our models we adopt a value of 0.01, which correspond to a thermal broadening of 20-30 km/s), ρ/ρ_{c*} is an output of the ADM model corresponding to the scaled density (where the scaling factor is $\rho_{c*} = M_{B=0}/4\pi R_*^2 v_e$), and w_z is the line-of-sight component of the velocity (in units of v_∞). The ADM model actually uses two different density scalings for the upflow and downflow components (ρ_{c*} and ρ_{w*}), but they are easily related by using the γ_w parameter, which for now is set at the canonical value of 2.6.

Furthermore, given the scope of this study, we limit our investigation to the absorption due to the intervening material which is in front of the stellar disk, along the line of sight. This is suitable to model the high velocity absorption trough, which is nearly unaffected by light that is scattered back into the line of sight. Future efforts will, however, take into account the full radiative transfer solution. For that same reason, we do not need to take into account a base photospheric absorption profile.

From the perspective of radiative transfer, using an analytic prescription to model the magnetospheric structure yields the marked advantage of allowing us to preset our integration grid, and then in a single loop both calculate the model at those points and integrate over each ray. This leads to a very efficient line synthesis technique, ideal for a vast parameter study.

We compute the absorption along 317 rays covering the stellar disk, where each ray contains 1000 linearly spaced points along the line of sight. The optical depth is computed along each ray using a piecewise linear integration scheme.

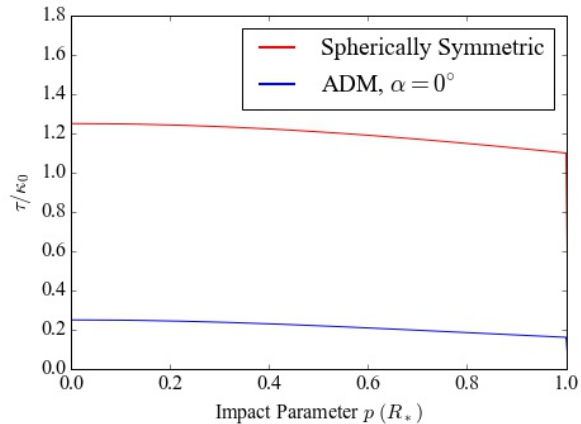


Figure 5. Optical depth at the stellar surface (scaled to the line strength, κ_0) as a function of the impact parameter p (scaled to the stellar radius, R_*) at $v/v_\infty = -0.8$, comparing a spherically symmetric outflowing stellar wind (red) with material trapped by a dipolar magnetic field viewed along the magnetic pole (blue). The decrease in optical depth between the spherically symmetric wind and the magnetized wind is immediately apparent, demonstrating that the presence of a magnetic field leads to the desaturation of the absorption trough observed in NGC 1624-2.

4.5 Modelling results

First, we illustrate the strong desaturation that occurs at high velocity at a given line strength. We computed the optical depth for each of the rays for a specific frequency and created surface maps for two specific cases: a spherically symmetric wind, and a wind threaded by a pure dipole seen pole-on. The result can be seen in Fig. 5. We chose a value of $w_{\text{obs}} = -0.8$, in the high-velocity absorption trough of the line. The optical depth is normalized to κ_0 . We can see that the magnetized wind has a much weaker optical depth at high velocity compared to the radially outflowing one. This corresponds to an effect that has already been observed for magnetic massive stars (see Fig. 3).

While this further demonstrates that spherically symmetric models are not suitable to infer wind properties from magnetic massive stars, it remains to be seen whether the ADM model can provide a quantitative approach to measure the wind-feeding rate of these objects. As a first proof of concept, we compute absorption-only line profiles and compare them to the pole-on spectrum of NGC 1624-2 and the CMFGEN model shown in Fig. 1. We model the strong CIV doublet, which is typically used to diagnose wind parameters.

To do so, we must first compute the line strength (κ_0) associated to the computed theoretical wind-feeding rate of NGC 1624-2. As in Wade et al. (2012a), we use a wind-feeding rate of $\log(\dot{M}_{B=0}) = -6.8$. Since the ADM model does not provide any information regarding ionization states throughout the magnetosphere, we have to resort to using the ion fraction outputted by the CMFGEN model, in this case $\log(n_{\text{CIV}}/n_{\text{H}}) \sim -5$. This leads to a value of $\kappa_0 = 5$.

Then, we validated this line strength value by comparing a profile obtained for a spherically symmetric outflow to the CMFGEN model presented in Section 4.2. We com-

puted profiles both with and without emission to determine at what velocity emission starts contributing significantly to the line profile; we found its contribution to be negligible for velocities ranging from $w_z = -1.0$ to $w_z = -0.8$.

We finally used the same line strength to compute a line profile (absorption only) using the ADM model viewed pole-on ($\alpha = 0^\circ$). The results are shown in Fig. 6. We can see that at high blue-shifted velocities (beyond $w_z = -0.8$), our spherically symmetric model is consistent with the CMFGEN model. Interestingly, the ADM model that we computed also seems to reproduce the high velocity line depth of the actual pole-on data, at least beyond $w_z = -0.9$. The discrepancy which arises at lower velocities obviously stems from the lack of emission in our profile, but could also be due to the magnetic geometry of NGC 1624-2: if the high state corresponds to a slightly off-pole view, this would lead to an even shallower absorption trough. For comparison, we also computed another ADM model line profile with a smaller line strength of $\kappa_0 = 0.5$, corresponding to an order of magnitude lower wind-feeding rate, similar to what a fit of the data to a spherically symmetric model would have yielded. The absorption in the latter model is shallower than the observed spectrum, even without any emission included, suggesting that such a rate is smaller than the actual wind-feeding rate of the star.

While this preliminary result does not allow us to place very strong constraints on the actual value of the wind-feeding rate, it does suggest that the observed UV spectrum of NGC 1624-2 is not inconsistent with the theoretical value computed by Wade et al. (2012a).

5 CONCLUSIONS

NGC 1624-2 exhibits remarkable variations in the profiles of its wind-sensitive UV resonance lines. These changes are much larger than those seen in other magnetic massive stars. In particular, the variations in its C IV and Si IV offer interesting parallels with behaviours previously noted in other magnetic stars, but also show some distinct characteristics, in particular the redshifted absorption that can be seen in the low state spectrum as well as the double-peaked emission in Si IV in the high-state spectrum.

Compared to MHD simulations, the ADM model offers a computationally inexpensive alternative which is much better suited for large parameter studies. As such, deriving wind parameters using the ADM formalism becomes a tractable problem, as opposed to simply providing a qualitative explanation for the line morphology. Admittedly, there might be some important limitations associated with the assumptions made by the ADM model⁹, but a more systematic study attempting to fit observational data with synthetic line profiles will help verify and refine these assumptions.

One difficulty in interpreting the variations seen in the spectra of various magnetic O stars comes from the uncertainties in the viewing angle of the magnetosphere (α).

⁹ One particular limitation of the ADM formalism, in the context of the faster-than-radial divergence which occurs at the pole and helps explain the strong line desaturation at high velocity, is that the resulting lower density along the magnetic pole is not taken into account dynamically, since a simple β -velocity law is used and no forces are being computed.

While our current understanding is that the optical high state corresponds to the smallest viewing angle (closest to magnetic pole-on) and that the low state corresponds to the largest viewing angle (closest to magnetic equator-on), comparing these observations to models will require more precise determinations of these viewing angles, and therefore better magnetic characterizations of these stars. This is not an easy undertaking as they are all slow rotators, but dedicated observing runs to fill in the phase coverage will ultimately prove necessary to better reconcile data and theory.

Within the limited scope of this paper, we have used the ADM model to produce synthetic UV line profiles which we have then compared to the data and to a CMFGEN model. The latter suggests that a low metallicity and microturbulent velocity are needed to reproduce the iron “forests”. We have limited our modelling with the ADM to the absorption component of the line, which is suitable to reproduce line depth at high velocities, in an effort to quantitatively characterize the wind-feeding rate of NGC 1624-2. We find that using a non-spherically symmetric model, we can attribute the desaturation of the line at high velocity to the magnetospheric geometry without having to involve atypically low wind-feeding rates. This means that we find our high-state observation to be consistent with the theoretical wind-feeding rate inferred by Wade et al. (2012a). This constitutes a proof of concept as to the quantitative potential of the ADM formalism and its potential to yield a useful means of analysis of UV spectra for magnetic O stars, thus laying the foundation for upcoming efforts.

Many improvements to our current modelling tools are being developed, including the full treatment of both the ADM model (including the downflow and shock retreat components, and allowing for a finite Alfvén radius) and radiative transfer (accounting for the “emission”, or more accurately the light that is scattered into the line of sight). This will constitute the basis for an in-depth parameter study to investigate the full range of UV line profile behaviours (Erba et al., in prep.). These new developments will also help us validate and, as needed, fine-tune the ADM formalism for quantitative UV spectral analysis.

Further improvements could also take into account doublets, for a precise modelling of the C IV doublet for instance, as well as a varying line strength as a function of the ionization fraction throughout the wind.

ACKNOWLEDGMENTS

This paper is dedicated to the memory of our wonderful colleague and co-author, Dr. Nolan Walborn, who recently passed away. Much of this study would not have been possible had it not been for his pioneering work in spectral classification and on the Of?p class of magnetic massive stars, as well as his constant efforts to obtain UV spectroscopy of these stars.

The authors would like to thank the reviewer (Prof. I. Howarth) for his helpful comments.

This research is based on observations made with the NASA/ESA *Hubble Space Telescope*, which is operated by the Association of Universities for Research in Astronomy, Inc., under NASA contract NAGS 5-26555. Support for *HST* General Observer Program number GO-13734 was provided

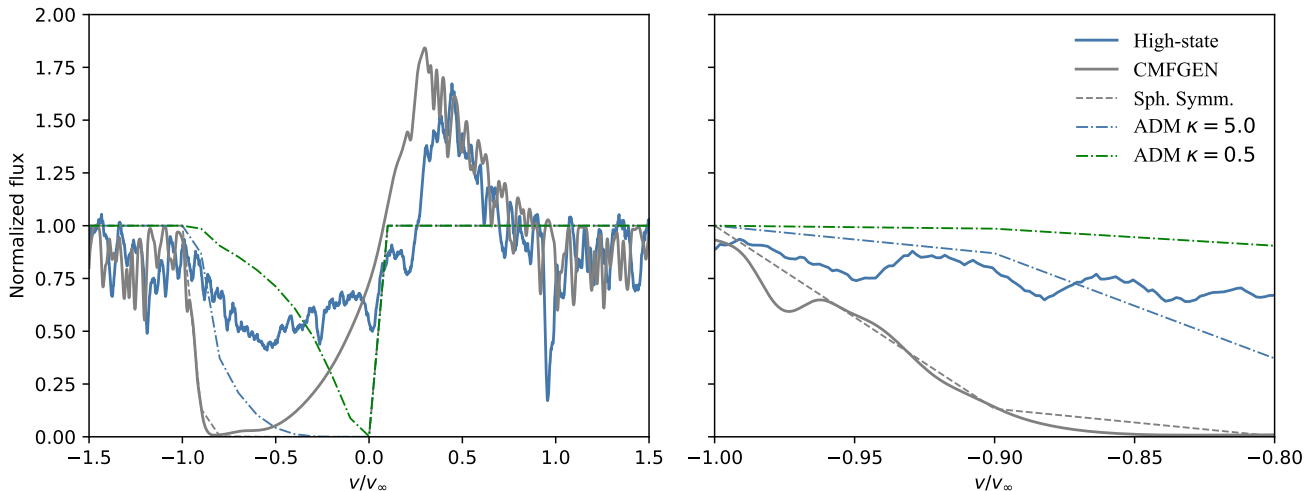


Figure 6. Comparison between the line profiles of the CIV doublet of NGC 1624-2 (high state, in solid blue), the CMFGEN model (in solid grey) computed using the theoretical mass-loss rate derived by Wade et al. (2012a) (see Section 4.2), and our absorption-only singlet model calculations using both a spherically symmetric wind (in dashed grey) and the ADM prescription (for line strengths corresponding to the theoretical wind-feeding rate in dash-dotted blue, and a wind-feeding rate which is one order of magnitude smaller in dash-dotted green). All profiles are normalized to their respective empirical or theoretical terminal velocity. The left panel shows the full line profiles, while the right panel focuses on the high-velocity blue-shifted absorption trough. As expected, there is good agreement between the CMFGEN model and our spherically symmetric model. In addition, the ADM profile with a line strength of $\kappa_0 = 5$ closely follows the observations of NGC 1624-2 in this regime (the departure at lower velocities is due to the missing emission in our model), while the ADM profile with a weaker line strength does not produce enough absorption to match the observation, even at lower velocities despite the lack of emission in the model.

by NASA through a grant from the Space Telescope Science Institute.

Support for this work was provided by NASA through Chandra Award G03-14017C issued by the Chandra X-ray Observatory Center which is operated by the Smithsonian Astrophysical Observatory for and behalf of NASA under contract NAS8-03060.

ADU gratefully acknowledges the support of the *Fonds québécois de la recherche sur la nature et les technologies* and of the Natural Science and Engineering Research Council (NSERC) of Canada, as well as support from program HST-GO-15066.001-A that was provided by NASA through a grant from the Space Telescope Science Institute, which is operated by the Association of Universities for Research in Astronomy, Inc., under NASA contract NAS 5-26555.

CE acknowledges graduate assistant salary support from the Bartol Research Institute in the Department of Physics, University of Delaware, as well as support from program HST-GO-13629.002-A that was provided by NASA through a grant from the Space Telescope Science Institute.

JMA acknowledges support from the Spanish Government Ministerio de Economía, Industria y Competitividad (MINECO/FEDER) through grant AYA2016-75 931-C2-2-P.

YN acknowledges support from the Fonds National de la Recherche Scientifique (Belgium), the Communauté Française de Belgique, and the PRODEX XMM contract.

AuD acknowledges support by NASA through Chandra Award numbers GO5-16005X and TM7-18001X issued by the Chandra X-ray Observatory Center which is operated by the Smithsonian Astrophysical Observatory for and on behalf of NASA under contract NAS8-03060.

GAW acknowledges Discovery Grant support from NSERC.

REFERENCES

- Carneiro L. P., Puls J., Sundqvist J. O., Hoffmann T. L., 2016, *A&A*, 590, A88
- Castro N. et al., 2015, *A&A*, 581, A81
- Danforth C. W., Keeney B. A., Stocke J. T., Shull J. M., Yao Y., 2010, *ApJ*, 720, 976
- Figer D. F. et al., 2002, *ApJ*, 581, 258
- Georgy C., Meynet G., Ekström S., Wade G. A., Petit V., Keszthelyi Z., Hirschi R., 2017, *A&A*, 599, L5
- Gräfener G., Koesterke L., Hamann W.-R., 2002, *A&A*, 387, 244
- Grunhut J. H. et al., 2009, *MNRAS*, 400, L94
- Grunhut J. H. et al., 2017, *MNRAS*, 465, 2432
- Grunhut J. H. et al., 2012, *MNRAS*, 426, 2208
- Hamann W.-R., 1981, *A&A*, 93, 353
- Hamann W.-R., Gräfener G., 2003, *A&A*, 410, 993
- Hennicker L., Puls J., Kee N. D., Sundqvist J. O., 2018, *A&A*, 616, A140
- Hillier D. J., Miller D. L., 1998, *ApJ*, 496, 407
- Howarth I. D. et al., 2007, *MNRAS*, 381, 433
- Keszthelyi Z., Wade G. A., Petit V., 2017, in Eldridge J. J., Bray J. C., McClelland L. A. S., Xiao L., eds, IAU Symposium Vol. 329, The Lives and Death-Throes of Massive Stars. pp 250–254
- Kopp R. A., Holzer T. E., 1976, *Sol. Phys.*, 49, 43
- Lamers H. J. G. L. M., Cerruti-Sola M., Perinotto M., 1987, *ApJ*, 314, 726

- Lamers H. J. G. L. M., Snow T. P., Lindholm D. M., 1995, *ApJ*, 455, 269
- Lanz T., Hubeny I., 2003, *ApJS*, 146, 417
- Marcolino W. L. F., Bouret J.-C., Sundqvist J. O., Walborn N. R., Fullerton A. W., Howarth I. D., Wade G. A., ud-Doula A., 2013, *MNRAS*, 431, 2253
- Marcolino W. L. F. et al., 2012, *MNRAS*, 422, 2314
- Martins F., Donati J., Marcolino W. L. F., Bouret J., Wade G. A., Escolano C., Howarth I. D., 2010, *MNRAS*, 407, 1423
- Martins F., Escolano C., Wade G. A., Donati J. F., Bouret J. C., Mimes Collaboration 2012, *A&A*, 538, A29
- Mayer P. et al., 2017, *A&A*, 600, A33
- Morel T. et al., 2015, in Meynet G., Georgy C., Groh J., Stee P., eds, IAU Symposium Vol. 307, New Windows on Massive Stars. pp 342–347
- Nazé Y., Petit V., Rinbrand M., Cohen D., Owocki S., ud-Doula A., Wade G. A., 2014, *ApJS*, 215, 10
- Nazé Y., Sundqvist J. O., Fullerton A. W., ud-Doula A., Wade G. A., Rauw G., Walborn N. R., 2015, *MNRAS*, 452, 2641
- Nazé Y., Walborn N. R., Rauw G., Martins F., Pollock A. M. T., Bond H. E., 2008, *AJ*, 135, 1946
- Owocki S. P., ud-Doula A., 2004, *ApJ*, 600, 1004
- Owocki S. P., ud-Doula A., Sundqvist J. O., Petit V., Cohen D. H., Townsend R. H. D., 2016, *MNRAS*, 462, 3830
- Pauldrach A. W. A., Kudritzki R. P., Puls J., Butler K., Hunsinger J., 1994, *A&A*, 283, 525
- Petit V. et al., 2015, *MNRAS*, 453, 3288
- Petit V. et al., 2017, *MNRAS*, 466, 1052
- Puls J., Urbaneja M. A., Venero R., Repolust T., Springmann U., Jokuthy A., Mokiem M. R., 2005, *A&A*, 435, 669
- Shenar T. et al., 2017, *A&A*, 606, A91
- Shultz M., Wade G. A., 2017, *MNRAS*, 468, 3985
- Simón-Díaz S., Herrero A., Esteban C., Najarro F., 2006, *A&A*, 448, 351
- Sota A., Maíz Apellániz J., Morrell N. I., Barbá R. H., Walborn N. R., Gamen R. C., Arias J. I., Alfaro E. J., 2014, *ApJS*, 211, 10
- Sota A., Maíz Apellániz J., Walborn N. R., Alfaro E. J., Barbá R. H., Morrell N. I., Gamen R. C., Arias J. I., 2011, *ApJS*, 193, 24
- Stahl O. et al., 1996, *A&A*, 312, 539
- Stibbs D. W. N., 1950, *MNRAS*, 110, 395
- Sundqvist J. O., Petit V., Owocki S. P., Wade G. A., Puls J., MiMeS Collaboration 2013, *MNRAS*, 433, 2497
- Sundqvist J. O., Puls J., Owocki S. P., 2014, *A&A*, 568, A59
- ud-Doula A., 2008, in Hamann W.-R., Feldmeier A., Oskinnova L. M., eds, Clumping in Hot-Star Winds. p. 125
- ud-Doula A., Owocki S. P., 2002, *ApJ*, 576, 413
- ud-Doula A., Owocki S. P., Townsend R. H. D., 2008, *MNRAS*, 385, 97
- ud-Doula A., Owocki S. P., Townsend R. H. D., 2009, *MNRAS*, 392, 1022
- Vink J. S., de Koter A., Lamers H. J. G. L. M., 2001, *A&A*, 369, 574
- Wade G. A. et al., 2012a, *MNRAS*, 425, 1278
- Wade G. A. et al., 2015, *MNRAS*, 447, 2551
- Wade G. A., Fullerton A. W., Donati J.-F., Landstreet J. D., Petit P., Strasser S., 2006, *A&A*, 451, 195
- Wade G. A. et al., 2012b, *MNRAS*, 419, 2459
- Wade G. A. et al., 2011, *MNRAS*, 416, 3160
- Wade G. A. et al., 2016, *MNRAS*, 456, 2
- Walborn N. R., 1972, *AJ*, 77, 312
- Walborn N. R., Nichols-Bohlin J., Panek R. J., 1985, NASA Reference Publication, 1155
- Walborn N. R., Sota A., Maíz Apellániz J., Alfaro E. J., Morrell N. I., Barbá R. H., Arias J. I., Gamen R. C., 2010, *ApJ*, 711, L143

APPENDIX A: LIST OF OBSERVATIONS

The table below provides a list of all the UV spectroscopic observations of non-magnetic and magnetic OB stars shown in Fig. 2 and Fig. 3, respectively.

Table A1. Full list of IUE and HST observations of the comparison non-magnetic and magnetic O stars used to produce, respectively, Fig. 2 and Fig. 3.

Star	Data ID	Telescope	Instrument	Exposure time (s)	Observation start time (UT)	Phase	Program ID and PI
HD 93146	SWP11136	IUE	SWP	3600	1981-01-24 01:43:07	N/A	OD40B (J.E. Hesser)
HD 36861	SWP46257	IUE	SWP	20	1992-11-13 06:25:36	N/A	SWOJN (J.S. Nichols)
HD 108	SWP08352	IUE	SWP	3300	1980-03-24 23:06:54	$\sim 0.0?$	NSCAD (A.K. Dupree)
	OBIL05010	HST	STIS	700	2010-09-09 16:15:11	$\sim 0.5?$	12179 (J.-C. Bouret)
HD 191612	OBIL01010	HST	STIS	1500	2010-08-23 01:53:54	0.751	12179 (J.-C. Bouret)
	OBIL02010	HST	STIS	1500	2011-01-04 06:49:30	0.000	12179 (J.-C. Bouret)
	OBIL03010	HST	STIS	1500	2011-05-18 06:38:32	0.250	12179 (J.-C. Bouret)
	OBIL04010	HST	STIS	1500	2011-09-30 12:02:56	0.501	12179 (J.-C. Bouret)
CPD -28 2561	OCI7A1010	HST	STIS	2110	2014-04-27 20:42:35	0.01	13629 (Y. Nazé)
	OCI7A3010	HST	STIS	2000	2014-05-15 07:58:15	0.25	13629 (Y. Nazé)
	OCI7A2010	HST	STIS	1850	2014-06-01 20:11:45	0.49	13629 (Y. Nazé)
HD 37022	SWP13737	IUE	SWP	60	1981-04-17 01:31:52	0.756	HSDRP (R.J. Panek)
	SWP14665	IUE	SWP	90	1981-08-05 19:12:21	0.936	LB304 (L. Bianchi)
	SWP54001	IUE	SWP	120	1995-03-01 03:49:56	0.256	RA110 (O. Stahl)
	SWP54040	IUE	SWP	100	1995-03-05 03:36:57	0.513	RA110 (O. Stahl)
	SWP54112	IUE	SWP	100	1995-03-13 04:06:57	0.033	RA110 (O. Stahl)
HD 57682	SWP03576	IUE	SWP	356	1978-12-12 06:29:00	0.671	RSLWK (L.W. Kamp)
	SWP21587	IUE	SWP	180	1983-11-20 07:51:44	0.050	MLFCG (C.D. Garmany)
HD 148937	SWP02893	IUE	SWP	3600	1978-10-09 05:56:00	0.462	OSPSC (P.S. Conti)
	O6F301010	HST	STIS	883	2001-09-16 20:39:44	0.959	9243 (A. Boggess)
HD 54879	OD3J01010	HST	STIS	383	2016-04-30 04:01:32	??	14480 (W.-R. Hamann)